

On the Generalization of the Kruskal-Szekeres Coordinates: A Global Conformal Charting of the Reissner–Nordström Spacetime

Fawzi Aly* and Dejan Stojkovic†
HEPCOS, Physics Department, SUNY at Buffalo, Buffalo, New York, USA

The Kruskal-Szekeres coordinate construction for the Schwarzschild spacetime could be interpreted simply as a squeezing of the t -line into a single point, at the event horizon $r = 2M$. Starting from this perspective, we extend the Kruskal charting to spacetimes with two horizons, in particular the Reissner-Nordström manifold, \mathcal{M}_{RN} . We develop a new method to construct Kruskal-like coordinates through casting the metric in new null coordinates, and find two algebraically distinct ways to chart \mathcal{M}_{RN} . We pedagogically illustrate our method by crafting two compact, conformal, and global coordinate systems labeled $\mathcal{GK}_{\mathcal{I}}$ and $\mathcal{GK}_{\mathcal{II}}$ as an example for each class respectively, and plot the corresponding Penrose diagrams. In both coordinates, the metric differentiability can be promoted to C^∞ in a straightforward way. Finally, the conformal metric factor can be written explicitly in terms of the t and r functions for both types of charts. We also argued that the chart recently reported in [1] could be viewed as a type-II chart.

I. INTRODUCTION

Reissner–Nordström (RN) spacetime is a unique, static, spherically symmetric, and asymptotically flat solution to the coupled set of Maxwell equations and Einstein field equations. It describes spacetime with the mass M , measured in the asymptotic region, and a static spherical electric field sourced by the charge Q in the background, with the corresponding nonzero stress energy tensor. Spherical-like coordinates, (t, r, θ, ϕ) , known as the Reissner–Nordström coordinates are the natural coordinates to represent the metric tensor $g_{\mu\nu}$ [2–6]. This chart could be assigned to an asymptotic observer, say Bob, at $r \rightarrow \infty$ equipped with a clock measuring the coordinate t . The RN metric in natural units ($c = G = 1$) can be written as

$$ds_{RN}^2 = \frac{-(r - r_+)(r - r_-)}{r^2} dt^2 + \frac{r^2 dr^2}{(r - r_+)(r - r_-)} \quad (1)$$

$$+ r^2 (d\theta^2 + \sin^2 \theta d\phi^2).$$

This coordinate system is ill-defined at two null hypersurfaces. Similar to the Schwarzschild spacetime, the coordinate singularity, at which $g_{tt} = 0$; locates the Killing horizons of the spacetime related to the Killing vector ∂_t .

$$g_{tt}(r_\pm) = 0, \quad (2)$$

$$r_\pm = M \pm \sqrt{M^2 - Q^2}.$$

For the non-extremal case, $M > Q$, the Reissner–Nordström black hole has an inner r_- and outer r_+ horizon, which makes its interior somewhat similar to the interior of the Kerr Spacetime [7, 8]. Further, in these coordinates the region $E_- = \{r | 0 < r < r_-\}$ the metric will have the same signature as in the region

$E_+ = \{r | r_+ < r < \infty\}$. Consequently, the physical point-like singularity at $r = 0$ is timelike in nature, in disagreement with the Schwarzschild spacelike singularity. The metric is dynamical in the trapped and anti-trapped regions $E = \{r | r_- < r < r_+\}$ (if we consider the maximal analytical extension of the RN manifold), since the r coordinate becomes timelike due to the flip of the metric signature in these coordinates [5].

We can easily illustrate the inconvenience of this chart in proximity to the RN’s black hole event horizon. Let us examine Bob’s clock, which times his girlfriend Alice’s trip, who is for some mysterious reasons, freely falling towards the outer horizon. While Alice measures a finite amount of time, $\Delta\tau$, using her own clock in her rest frame, Bob measures a significantly dilated duration of time, Δt , by timing Alice’s worldline. In other words, Bob will never see Alice crossing the outer event horizon in his lifetime. Generically, timelike (spacelike) intervals suffer from infinite dilation (contraction) once measured near the RN’s horizons using Bob charting devices. Therefore, better charts are needed to describe phenomena where Bob’s tools fail [9].

Finding a new charting system to describe regions near and across the null hypersurfaces in different spacetimes is a long-standing business. Novikov coordinates [10], Lemaître coordinates [11], Gullstrand–Painlevé coordinates [12, 13], Eddington–Finkelstein coordinates [14], and Kruskal–Szekeres coordinates [15–17] are all examples of charts developed to overcome the incompetents of the Schwarzschild coordinates near its event horizon located at $r = 2M$ where M is the Schwarzschild BH mass. Some of them have been generalized to Reissner–Nordström [4] and Kerr spacetimes [18, 19]. Most of them were constructed by studying timelike and null-like geodesics behavior around the blackhole. However, we decided to follow a different and more algebraic approach to find new global charts, relying on the simplest mathematical way to interpret what define a good coordinate. Our argument is analogous to the one found in

* [mabbasal\[AT\]buffalo.edu](mailto:mabbasal[AT]buffalo.edu)

† [ds77\[AT\]buffalo.edu](mailto:ds77[AT]buffalo.edu)

[9].

Although astrophysical black holes are expected to be electrically neutral [20], even a small amount of charge on a large black hole could be important when we encounter certain phenomena such as cosmic rays [21]. Also, small primordial black holes that did not live long enough to get neutralized can carry a significant amount of charge. Another exception might be black holes charged under some other hidden $U(1)$ gauge group different from electromagnetism [22, 23]. This provides enough motivation to study RN black holes not only for academic interests but also from a phenomenological point of view. On the other hand, studying the causal structure of the RN black hole, which is entirely different from the one associated with the Schwarzschild spacetime, is important also as it shares some generic features with other types of black holes with two horizons, e.g. the Kerr black hole which is much more relevant in astrophysical situations [8, 24].

Klösch and Strobl managed to provide *non-conformal* global coordinates for the extreme and non-extreme RN spacetimes [25]. Moreover, most of the attempts to construct conformal global coordinates were based on patching two sets of the Kruskal-Szekeres coordinates \mathcal{K}_\pm , where each set is well-behaved on one horizon r_\pm while it fails on the other one r_\mp . This makes the region of validity for each chart $\mathcal{E}_+ = E_+ \cup \{r|r_- < r \leq r_+\}$ and $\mathcal{E}_- = E_- \cup \{r|r_- \leq r < r_+\}$ respectively. Switching between the two charts was the key to covering the whole RN manifold and constructing a global Penrose diagram in [24, 26, 27]. Such patched Penrose diagrams, found in [5] for example, will still prove inconvenient if we want to study geodesics across the horizons [28, 29]. To overcome this obstacle, a global conformal coordinate system is required.

Recently in [1], Farshid proposed a *smoothing* technique that could be used to provide a C^2 -conformal global chart for the RN spacetime, and pointed out the possibility of generalizing the method to spherically symmetric spacetimes. The used method was reported to be a generalization of one used by Andrew Hamilton in [24] aiming to promote the differentiability of the map. One can also find Penrose diagrams constructed using this method in [29]. The central idea of this work was to find coordinates that extrapolate to each of the Kruskal-Szekeres coordinates \mathcal{K}_\pm when approaching the horizon located at $r = r_\pm$. In addition, smoothing was achieved through the use of the bump functions [30, 31]. A similar technique was used by Schindler in [32, 33] to overcome the limitations of the Carter method of charting two-horizons spacetimes [26]. This technique was designed to provide a global chart regular for a special class of spherically symmetric spacetimes with multiple horizons defined in the work as the *Strong Spherical Symmetric* spacetimes. The reader can also find a comprehensive summary of the Penrose diagram theory in the chapter

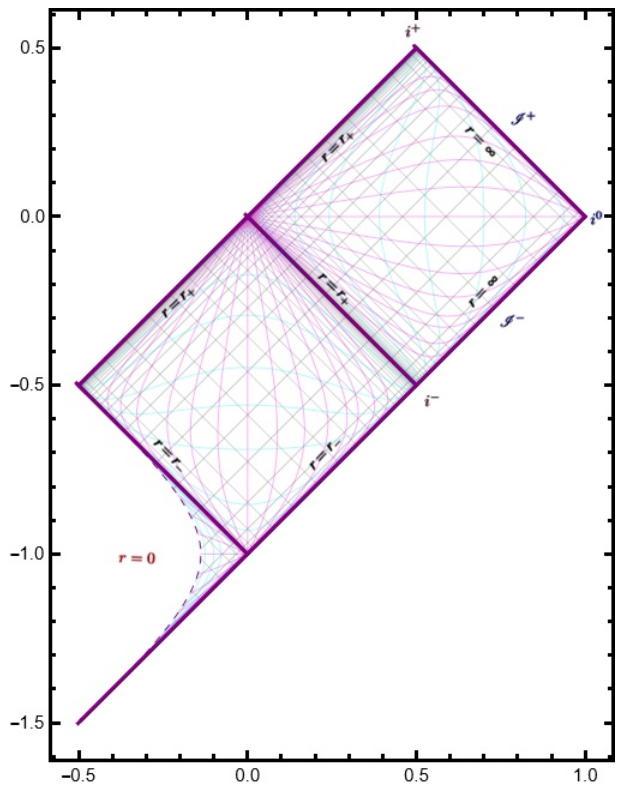


FIG. 1. Penrose Diagram for a single Reissner Nordstrom ($M = 1, Q = .96$) Universe constructed using the example for Type-I coordinates given in IV A. The Kruskal coordinates (T, R) are plotted on the y-axis and x-axis respectively. The constant- r and constant- t curves are plotted in cyan and magenta while the null-geodesics are plotted in gray. The outer r_+ and inner r_- horizons are described by $T = \pm R$ and $T = \pm R - 1$ lines. The physical singularity at $r = 0$ is plotted as a curve in dashed purple.

one of Schindler's doctoral thesis [34].

In this work, we will define a new procedure that can produce compact, conformal, and global (CCG) charts that are valid at both the inner and outer horizons of RN spacetime, and for which the metric could be infinitely differentiable C^∞ . Using this procedure we will cast the possible two CCG coordinate systems for the RN spacetime into two categories, which we label as type-I and type-II coordinates. The reader can find a Penrose diagram of a single and Block Universe of the RN spacetime in figure [1] and figure [2] constructed using examples of type-I and type-II CCGs respectively. Moreover, the coordinates provided in [1] could be thought of as coordinates of type-II. Our method makes no underlying assumptions about the nature of the spacetime, other than it should possess two horizons and that there exist some double null coordinates to chart it locally. Therefore, to facilitate future applications of this procedure, we will present here a detailed pedagogical approach.

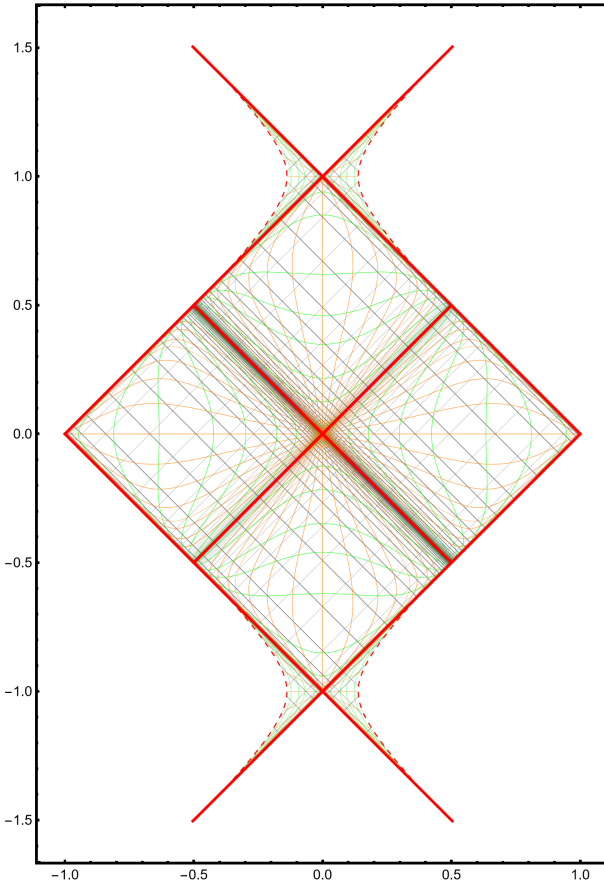


FIG. 2. Penrose Diagram for a block universe of Reissner-Nordstrom ($M = 1$, $Q = .96$) Universes using type-II coordinates found in IV B. The Kruskal coordinates (T, R) are plotted on the y -axis and x -axis respectively. The constant- r and constant- t curves are plotted in green and orange while the null-geodesics are plotted in gray. The outer r_+ and inner r_- horizons are described by $T = \pm R$ and $T = \pm R \pm 1$ lines, while the physical singularity at $r = 0$ is plotted as a red curve.

The structure of this paper is as follows. In section II A, we begin by reformulating the core idea of the Kruskal chart, and then revisit the Kruskal charting of the Schwarzschild II B and the RN II D spacetimes. In section III, the main procedure for constructing generalized Kruskal charts is presented. The type-I and type-II coordinates as well as their relaxed versions for RN spacetime are given in IV A and IV B. Finally, we discuss the outcome of the analysis and possible future work in section V. Also the reader can find an argument why Soltani's smoothing technique could be thought of Type-II chart in Appendix A, and an example on the relaxation step as an optional part of the procedure in Appendix B.

II. PRELIMINARY

A. Kruskal-Szekeres coordinates

Kruskal-Szekeres coordinates represent a maximal CCG chart for the Schwarzschild metric and has been studied extensively in the literature [15–17, 35, 36]. Their global nature is attributed to two features: (i) they can cover the null hypersurface located at radius $r = 2M$ which Bob will fail to chart, and (ii) it is a maximal extension of the Schwarzschild chart representing two copies of the Schwarzschild universe. The metric written in the spherical-like coordinate known as the Schwarzschild Spacetime (t, r, θ, ϕ) ¹ where $t \in \mathbb{R}$, $r \in \mathbb{R}_+ \setminus \{0\}$, $\theta \in (0, \pi)$, and $\phi \in [0, 2\pi)$ takes the well-known form

$$\begin{aligned} dS_{Sch}^2 &= \left(\frac{r - 2M}{r} \right) \{ -dt^2 + dr_*^2 \} \\ &= \frac{1}{r(r_*)} (r(r_*) - 2M) dS_{Con}^2, \end{aligned} \quad (3)$$

where dS_{Sch}^2 and dS_{Con}^2 stand for the Schwarzschild and conformal metric² respectively. Here, r_* is defined³ as follows

$$\exp(r_*) = \exp(r) |r - 2M|^{2M}. \quad (4)$$

It is worth emphasizing that the map from r -coordinate to its tortoise version r_* is bijective and its inverse is differentiable on each of \mathcal{S}_+ and \mathcal{S}_- separately as defined below. This is obviously due to the modulus included in the definition of these coordinates in equation (4).

A rigorous procedure would involve solving the Einstein Field Equations in Kruskal coordinates (which is the *top-down* approach as in [9, 37]⁴) by means of null-casting and the null gauge⁵. Since the Schwarzschild coordinates cover only the regions $\mathcal{S}_- = \{r | 0 < r < 2M\}$ and $\mathcal{S}_+ = \{r | 2M < r < \infty\}$ ⁶ of one universe of the Kruskal metric, trying to map the local chart to the global one (i.e. the *bottom-up* approach) is not quite rigorous, because the map between the two charts as well as

¹ Since examining the behavior and possible problems of the spherical coordinates as $r \rightarrow \infty$ falls beyond the scope of this work, the angular dependence (θ, ϕ) will be neglected from now on for simplicity.

² Conformal to 2D minkowskian manifold

³ Usually, the constant of integration in defining the tortoise coordinate, r_* , is chosen to be $-2M \ln(2M)$ in order to maintain dimensionless quantity inside the natural logarithm. Here, for simplicity, we omit this step.

⁴ The conformal factor in these references is written in terms of r , however, it is more instructive to think of $r(U, V)$ as a function of U and V , and not as the areal coordinate r .

⁵ freedom to redefine the null coordinates while preserving the null structure of the spacetime.

⁶ where only the attribution to an asymptotic observer is defined in the region \mathcal{S}_+ .

the Jacobian, Hessian, and the higher-versions of it will be singular at the event horizon [38].

Nevertheless, we seek a global chart in which the metric is at least C^2 everywhere on the manifold in order to satisfy the coupled Field Equations which contain first and second derivatives of the metric. Thus, we can apply this bottom-up approach (as in most of the General Relativity textbooks [3, 39]) by studying the limit at $r = 2M$ and analytically continuing the metric there. Finally, the metric $g_{\mu\nu}$ must be written explicitly in the Kruskal coordinates (T, R, θ, ϕ) only. In this paper, we will follow the bottom-up approach to find the generalized Kruskal coordinates which chart the whole RN spacetime. Taking the Kruskal charting of the Schwarzschild black hole as our guide, we review the traditional derivation of the Kruskal coordinates.

B. Construction of the Kruskal coordinates: Schwarzschild Spacetime

We begin by mapping the Schwarzschild coordinates to intermediate null coordinates first, in particular the retarded (u) and advanced (v) time coordinates, defined as $u = t - r_*$ and $v = t + r_*$. To handle the coordinate singularity of the former at the horizon, $r = 2M$, the null freedom is used to map the latter set to another set of the null coordinates using $u \rightarrow U \equiv h(u)$ and $v \rightarrow V \equiv k(v)$. This gives

$$dS_{con}^2 = -dudv = -\frac{dUdV}{\frac{dh}{du} \frac{dk}{dv}} \equiv -\frac{Q(U, V)dUdV}{r(U, V) - 2M}, \quad (5)$$

where $Q(U, V)$ is at least C^2 -function $\mathcal{S} = \mathcal{S}_+ \cup \mathcal{S}_- \cup \{r|r = 2M\}$. This is achieved by employing the definition of r_* . A sufficient coordinate transformation is given by

$$U \equiv \nu \exp\left(\frac{-u}{4M}\right), \quad V \equiv \nu \exp\left(\frac{v}{4M}\right), \quad (6)$$

where

$$\nu = \begin{cases} +1 & r > 2M \\ -1 & r < 2M \end{cases}, \quad (7)$$

The signs \pm are included to achieve the maximal analytical extension of the metric. The product UV is positive in the regions II and III, and negative in the regions I and IV, following the convention given in [3]. The r coordinate is defined implicitly as

$$UV = \exp\left(\frac{r}{2M}\right)(r - 2M). \quad (8)$$

This equation can be explicitly solved for r by employing the multi-valued Lambert function W [40, 41],

$$r = 2M \left[W\left(\frac{UV}{-2Me}\right) + 1 \right]. \quad (9)$$

where e is the Euler number. Then, the Schwarzschild metric will have the following form in the new double null coordinates

$$dS_{Sch}^2 = -\frac{16M^2e^{-\frac{2M}{r(U, V)}}}{r(U, V)}dUdV + r^2(U, V)d\Omega^2. \quad (10)$$

Finally, the Kruskal coordinates T_{KS} and R_{KS} are related to the new null coordinates through the following transformations

$$\begin{aligned} U &\equiv \frac{1}{2}(T_{KS} - R_{KS}), \\ V &\equiv \frac{1}{2}(T_{KS} + R_{KS}). \end{aligned} \quad (11)$$

It is worth writing the final version of the metric in the Kruskal coordinates as

$$\begin{aligned} dS_{Sch}^2 &= \omega(T_{KS}, R_{KS})(-dT_{KS}^2 + dR_{KS}^2) \\ &+ 4M^2(W(T_{KS}, R_{KS}) + 1)^2 d\Omega^2, \end{aligned} \quad (12)$$

where

$$\omega(T_{KS}, R_{KS}) = \frac{8M \exp[-W(T_{KS}, R_{KS}) - 1]}{W(T_{KS}, R_{KS}) + 1}. \quad (13)$$

As a cross-check, one could verify that the Einstein tensor $G_{\mu\nu}$ corresponding to the Kruskal metric is zero everywhere on the Schwarzschild manifold, thus confirming that the stress-energy tensor $T_{\mu\nu}$ is identically zero (as it must be for the Schwarzschild solution). This is true despite the fact that taking the derivatives of the metric with respect to the coordinates (T, R) (using implicit differentiation with respect to (t, r)) will be ill-defined at the event horizon. One could also verify that the maps between the Kruskal and the Schwarzschild chart are diffeomorphic in the regions \mathcal{S}_+ and \mathcal{S}_- [38].

C. A simple interpretation of the Kruskal charting

The procedure of constructing Kruskal coordinates for Schwarzschild spacetime outlined in the previous section becomes limited when applied to spacetimes with more than one horizon. To be able to resolve this obstacle, we re-interpret the main premise of the construction. If Bob lived in a four-dimensional Minkowski spacetime, his clock would be able to properly time the events taking place there globally. However, once the spacetime is only asymptotically Minkowskian, the chart will fail near the null hypersurfaces. We can illustrate this scenario through the cartoon shown in figure [3].

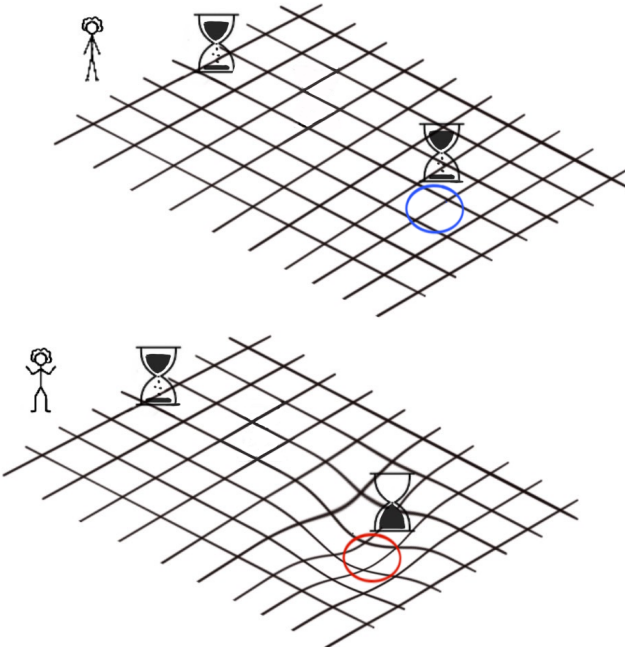


FIG. 3. Bob, an asymptotic observer; is trying to time out the duration of an event (or the time interval between two successive events) taking place in two different locations. In the upper picture, there is no curvature, and Bob's clock timed both events in finite and equal intervals of time. However, when Bob uses the same clock in the lower picture with a curved spacetime, the time interval keeps getting longer as the event take place near to the event horizon, until the interval becomes infinite exactly at the horizon (the red circle). Credit for this illustration to the artist Haidi Fawzi

But what if the charting method (the ruler and the clock) were ill-defined in a Minkowski spacetime at precisely these locations which correspond to the null hypersurfaces in a curved spacetime? For example, we can define a "bad" chart \mathcal{Z} in the conformal spacetime with the metric $g_{\mu\nu}^{Con}$, in which any given timing of $\Delta\tau$ of Alice's trip to the $r = 2M$ ⁷ is mapped to $\Delta\tilde{t} \rightarrow 0$. Apparently, there is a family of these "bad" charts \mathcal{Z} that would be well defined on the physical spacetime, with the metric $g_{\mu\nu} = \omega(x)g_{\mu\nu}^{Con}$, where $\omega(x)$ is the conformal factor. They are only conditioned to contract the time interval $\Delta\tau$ at the same rate as the dilation of time in Bob's frame. One can find an equivalent argument in [9] that we quote here "*A better coordinate system, one begins to believe, will take these two points at infinity and spread them out into a line in a new (r_{new}, t_{new}) -plane; and will squeeze the line ($r = 2M, t$ from $-\infty$ to ∞) into a single point in the (r_{new}, t_{new}) -plane*". A cartoon similar to figure [3] can be made for such clocks which we will name *Kruskal's clock* in figure [4]. In this step,

we are not associating such a chart with any particular observer.

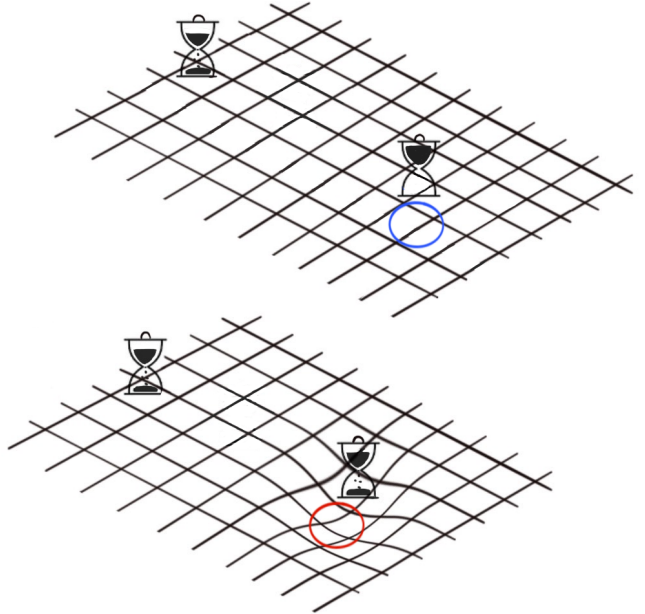


FIG. 4. In the upper flat spacetime, the clock is constructed in a way to squeeze the time interval to zero at the particular location where the horizon would be located in a curved spacetime (the blue circle). Consequently, if Bob used this weird clock in a flat universe, the measurements won't make any sense. However, if the same Kruskal's clock is used in the curved spacetime, it will report finite time intervals in proximity and across the horizon (the red circle). Credit for this illustration to the artist Haidi Fawzi

As we will show here later, applying this simple argument to spacetimes with more than one horizon would be a tedious algebraic task. Mathematically, the fundamental premise of the construction is to find conformal coordinates \mathcal{Z} that generate poles of the same rank as zeros of the conformal factor. Then in this bottom-up approach the zeros and poles cancel out, and the physical metric in \mathcal{Z} will be CCG. In the next subsections, we will review the Kruskal charting of the RN spacetime following the notation in [4, 24].

D. Outer and inner Kruskal coordinatse: Reissner-Nordstrom spacetime

One example where the standard Schwarzschild-like Kruskal charting will fail in constructing a CCG is the RN spacetime.

$$ds_{RN}^2 = \frac{(r - r_+)(r - r_-)}{r^2} \{ -dt^2 + dr_*^2 \} \quad (14)$$

$$= \frac{(r - r_+)(r - r_-)}{r^2} ds_{Con}^2,$$

⁷ In our analysis the conformal spacetime is Minkowski, so there are no horizons at the radius $r = 2M$.

where dS_{RN}^2 stands for RN metric, while (u, v) represents the double null coordinates constructed in the same manner as in the Schwarzschild case. The RN radial tortoise coordinate r_* is defined as

$$\begin{aligned} \exp(r_*) &= \exp(r) |r - r_+|^{\frac{\alpha_+}{2}} |r - r_-|^{-\frac{\alpha_-}{2}}, \\ \alpha_+ &\equiv \frac{2r_+^2}{r_+ - r_-}, \\ \alpha_- &\equiv \frac{2r_-^2}{r_+ - r_-}, \end{aligned} \quad (15)$$

where α_+ and α_- are the surfaces gravity at r_- and r_+ respectively.

Similar to the Schwarzschild tortoise coordinate, $r_*(r)$ is bijective and its inverse is differentiable on E_+ , E , and E_- separately. However, there is a potential to solve explicitly for r by employing generalized Lambert functions \mathcal{W} [42–45]. Since this is a tedious task on its own, we confine our analysis to the main objective, while this step could be addressed in future work.

By examining the tortoise coordinate definition, it is obvious that a zero at r_\pm is always coupled with a pole at r_\mp , hence it is not straightforward to factor out a product of simple poles at r_+ and r_- in the conformal metric. Nevertheless, it remains possible to construct regular charts at one horizon that is ill-defined at the other. These coordinates are regular in the domain \mathcal{E}_+ and \mathcal{E}_- , respectively. The outer \mathcal{K}_+ and inner \mathcal{K}_- Kruskal coordinates are simply related to the “-” null-chart $(\mathcal{U}_-, \mathcal{V}_-)$ and “+” null-chart $(\mathcal{U}_+, \mathcal{V}_+)$ following the similar but unitless definitions as those found in (11). We will work with the following sign convention

$$\begin{aligned} \mathcal{U}_+ &= \nu_+ U_+, & \mathcal{V}_+ &= \nu_+ V_+ \\ U_+ &= \exp\left(\frac{-u}{\alpha_+}\right), & V_+ &= \exp\left(\frac{v}{\alpha_+}\right), \end{aligned} \quad (16)$$

where

$$\nu_+ = \begin{cases} +1 & r > r_+ \\ -1 & r < r_+ \end{cases}, \quad (17)$$

to represent the maximal analytical extension of these coordinates. Then the t and r coordinates are characterized by the following curves in the $(\mathcal{U}_+, \mathcal{V}_+)$ -plane:

$$\begin{aligned} \mathcal{U}_+ \mathcal{V}_+ &= \exp\left(\frac{r}{2\alpha_+}\right) (r - r_+) |r - r_-|^{-\alpha}, \\ \frac{\mathcal{V}_+}{\mathcal{U}_+} &= \pm \exp\left(\frac{2t}{\alpha_+}\right). \end{aligned} \quad (18)$$

Similarly,

$$\begin{aligned} \mathcal{U}_- &= \nu_- U_-, & \mathcal{V}_- &= \nu_- V_-, \\ U_- &= \exp\left(\frac{u}{\alpha_-}\right), & V_- &= \exp\left(\frac{-v}{\alpha_-}\right) \end{aligned} \quad (19)$$

where

$$\nu_- = \begin{cases} +1 & r > r_- \\ -1 & r < r_- \end{cases}. \quad (20)$$

The t and r curves in the $(\mathcal{U}_-, \mathcal{V}_-)$ -plane are defined as

$$\begin{aligned} \mathcal{U}_- \mathcal{V}_- &= \exp\left(-\frac{r}{2\alpha_-}\right) (r - r_-) |r - r_+|^{-\bar{\alpha}}, \\ \frac{\mathcal{V}_-}{\mathcal{U}_-} &= \pm \exp\left(-\frac{2t}{\alpha_-}\right), \end{aligned} \quad (21)$$

Consequently, the metric in these “+” or “-” null-charts becomes

$$\begin{aligned} dS_{RN}^2 &= -\alpha \pm \frac{(r - r_+) (r - r_-)}{r^2} \frac{d\mathcal{U}_\pm d\mathcal{V}_\pm}{\mathcal{U}_\pm \mathcal{V}_\pm} \\ &= -\alpha_+ \frac{\exp\left(-\frac{2r}{\alpha_+}\right)}{r^2} (r - r_-)^{1+\alpha} d\mathcal{U}_+ d\mathcal{V}_+ x^a x^a \\ &= -\alpha_- \frac{\exp\left(\frac{2r}{\alpha_-}\right)}{r^2} (r_+ - r)^{1+\bar{\alpha}} d\mathcal{U}_- d\mathcal{V}_-, \end{aligned} \quad (22)$$

where⁸

$$\begin{aligned} \alpha &\equiv \frac{\alpha_-}{\alpha_+} = \left(\frac{r_-}{r_+}\right)^2 \rightarrow 0 < \alpha < 1, \\ \bar{\alpha} &\equiv \frac{\alpha_+}{\alpha_-} = \left(\frac{r_+}{r_-}\right)^2 \rightarrow 1 < \bar{\alpha}. \end{aligned} \quad (23)$$

It is easy to check that the metric in “+” (“-”) null-coordinates is regular at the outer (inner) horizon $r_+(r_-)$. However, the coordinates fail⁹ at the inner (outer) horizon $r_-(r_+)$. Moreover, the metric in the “+”-null coordinates is not asymptotically flat in agreement with the Schwarzschild induced metric defined on the hypersurfaces with fixed θ and ϕ in equation (12), where the conformal factor approaches zero as $r \rightarrow \infty$. Nevertheless, global Kruskal coordinates could be built by combining these two definitions in (16, 19) together (see e.g. the work of Carter [26], Hamilton [24] Schindler [32], and Farshid [1]). Although they all managed to find a regular metric across the horizon, yet the metric at maximum was only C^2 .

III. GLOBAL CONFORMAL CHART CRITERIA

We start our analysis by studying the conditions needed for a valid conformal global chart. We want

⁸ The extreme cases ($Q = M$ and $Q > M$) of the RN metric are not considered here.

⁹ $dS_{RN}^2 = 0$ at $r = r_-$ (r_+) in the “+” (“-”) coordinates according to equation (22).

to map the double null coordinates (u, v) to the global double null coordinates (\tilde{u}, \tilde{v}) . The most direct way to achieve that will be to use only the null gauge [46, 47] as follows

$$\begin{aligned}\tilde{u} \equiv h(u) \quad &\rightarrow \quad du = \frac{1}{dh} d\tilde{u}, \\ &\quad \frac{du}{dh} \\ \tilde{v} \equiv k(v) \quad &\rightarrow \quad dv = \frac{1}{dk} d\tilde{v}.\end{aligned}\quad (24)$$

To construct a well-defined chart on the entire Reissner–Nordström manifold, we identify three distinct possibilities with reference to the singularity structure of the term $\frac{dh}{du} \frac{dk}{dv}$, focusing on its behavior at $r = r_-$ and $r = r_+$. The three options are:

1. **Type-O:** $\frac{dh}{du} \frac{dk}{dv}$ has a zero either at $r = r_-$ or $r = r_+$. The regularity of the metric in the new (\tilde{u}, \tilde{v}) coordinates would be achieved at $r = r_-$ or $r = r_+$ but not simultaneously. “ \pm ” null coordinates are examples for this case. However, generating nontrivial coordinates out of (U_\pm, V_\pm) is possible¹⁰ ¹¹. This condition could be formulated as follows

$$\frac{dh}{du} \frac{dk}{dv} = (r - r_\pm) \zeta(r_*, t) \quad (25)$$

2. **Type-I:** $\frac{dh}{du} \frac{dk}{dv}$ has a product of zeros at $r = r_-$ and $r = r_+$.

If we manage to factor out this product of zeros while keeping the associated poles decoupled, then we will have a conformal global coordinate for the RN spacetime. We will illustrate this case with an example in IV A. This condition can be formulated as

$$\frac{dh}{du} \frac{dk}{dv} = (r - r_+) (r - r_-) \gamma(r_*, t) \quad (26)$$

3. **Type-II:** a sum of decoupled simple zeros at $r = r_+$ and $r = r_-$, each coupled to a pole, and possibly zeros of constrained rank at $r = r_-$ for former and $r = r_+$ for later. In principle, this mixture of poles and zeros might be easier to find compared to **Type-I**, however, the metric is expected to be more complicated form-wise. We will illustrate this

¹⁰ The transformations that lead to such coordinates are expected to be more complicated as they are restricted by the requirement to leave the singularity structure invariant or to generate a decoupled zero at the other horizon.

¹¹ For example, the transformation of the form $f(U) \equiv U^p$ and $g(V) \equiv V^p$ where $p \in \mathbb{R}$ are allowed since they clearly change the singularity structure of the term $\frac{dh}{du} \frac{dk}{dv}$.

case with an example in IV B. This condition can be formulated as

$$\begin{aligned}\frac{dh}{du} \frac{dk}{dv} = (r - r_+) M_+(r_*, t) + (r - r_-) M_-(r_*, t) \\ + \beta(r_*, t),\end{aligned}\quad (27)$$

The three differential equations listed above are sufficient to construct the desired singularity structure in each case, while the constraints are encoded within ζ , γ , M_\pm and β .

IV. CONSTRUCTING CCGS FOR REISSNER–NORDSTRÖM SPACETIME

A. Type-I CCG Global Chart

As we mentioned before, just by looking at the definition of r_* , there is no simple way of factorizing the zeros $(r - r_+)$ or $(r - r_-)$ without invoking poles at r_- or r_+ . Still, we can consider combining equations (21) and (18)

$$\mathcal{U}_+ \mathcal{U}_- \mathcal{V}_+ \mathcal{V}_- = \frac{(r - r_+)}{|r - r_+|^\alpha} \frac{(r - r_-)}{|r - r_-|^\alpha} \exp\left(\frac{r}{2\alpha_+} - \frac{r}{2\alpha_-}\right) \quad (28)$$

This may give us a hint for how to find (\tilde{u}, \tilde{v}) with the desired map to fulfill the singularity structure of type-I. For example, we can start with the following definitions of $\mathcal{GK}_\mathcal{I}$

$$\frac{dh}{du} = \frac{\mu_u}{U_+^{-1} + U_-^{-1}}, \quad \frac{dk}{dv} = \frac{\mu_v}{V_+^{-1} + V_-^{-1}}, \quad (29)$$

where we can define a sign function μ as

$$\mu = \begin{cases} +1 & r > r_+ \mid r < r_- \\ -1 & r_- < r < r_+ \end{cases} \quad (30)$$

The definition we give in (29) reduces to evaluating the I_1 -integration given here

$$I_1 = \int \frac{1}{x^q + 1} dx, \quad (31)$$

where $q > 1$. This integration has an upper and lower bound, hence the sign convention we use here will locate the inner horizon r_- , outer horizon r_+ and the asymptotically flat region $r \rightarrow \infty$ according to the choice of the reference point. We choose that point to be the outer horizon $u \rightarrow -\infty$ ($v \rightarrow \infty$). Accordingly, if we stick to the $\mu = \mu_v = \mu_u$ in (30), we can have a monotonic map from $u(v)$, defined in any of the regions E_\pm and E ; to \tilde{u} (\tilde{v}). However, as we want to explicitly chart one of the RN universe let's choose $\mu_v = 1$ while $\mu = \mu_u$. As the ODEs in (29) could be easily integrated in terms of the

Hypergeometric functions ${}_2F_1(a, b; c; x)$ [48–50].

$$\tilde{u} = \begin{cases} \frac{S_-(u)}{S_0} - 1 & r > r_+ \\ 1 - \frac{S_-(u)}{S_0} & r_+ > r > r_- \\ \frac{S_-(u)}{S_0} - 2 & r_- > r \end{cases} \quad (32)$$

and

$$\tilde{v} = \frac{S_+(v)}{S_0} - 1 \quad (33)$$

while

$$\begin{aligned} S_{\pm}(x) &= \alpha_{\pm} e^{\frac{x}{\alpha_{\pm}}} {}_2F_1(1, k_{\pm}, 1 + k_{\pm}, -e^{\kappa x}) \\ S_0 &= \max[S_{\pm}(x)] \end{aligned} \quad (34)$$

and

$$\begin{aligned} k_{\pm} &= \frac{\alpha_{\pm}}{\alpha_+ + \alpha_-} \\ \kappa &= \frac{1}{\alpha_+} + \frac{1}{\alpha_-} \end{aligned} \quad (35)$$

These coordinates have a *compact* domain and, hence, could be used directly to construct Penrose diagrams for the RN spacetime. The choice of signs μ_v and μ_u does not harm the continuity or differentiability of the map, still, it will cause signature flip of the metric once written in those Generalized null Kruskal Coordinate of type-I, however this is straightforwardly treatable by absorbing the signs while defining their (T_{KS}, R_{KS}) version. The function of μ_v and μ_u is simply to define the maximal analytical extension of RN manifold. The metric in the CCG type-I coordinates will take the following form:

$$\begin{aligned} dS_{RN}^2 &= -\mu_v \mu_u \frac{d\tilde{u} d\tilde{v}}{r^2} \left\{ |r - r_-|^{\alpha+1} \exp\left(-\frac{2r}{\alpha_+}\right) \right. \\ &+ |r - r_+|^{\bar{\alpha}+1} \exp\left(\frac{2r}{\alpha_-}\right) + 2 \cosh\left[t\left(\frac{1}{\alpha_+} + \frac{1}{\alpha_-}\right)\right] \\ &\times \exp\left(r\left[\frac{-1}{\alpha_+} + \frac{1}{\alpha_-}\right]\right) |r - r_+|^{\frac{\alpha+1}{2}} |r - r_-|^{\frac{\alpha+1}{2}} \left. \right\}. \end{aligned} \quad (36)$$

Using these coordinates a block Penrose diagram is constructed as shown in figure [5].

The metric possesses a conformal factor resembling the sum of the conformal factors of the \mathcal{K}_{\pm} in addition to a new time-dependent term that vanishes on both horizons. The metric is well-behaved on both of the horizons and takes the following asymptotic behavior as $r \rightarrow r_+$,

$$dS_{RN}^2(r \rightarrow r_+) \rightarrow -\frac{\exp\left(-\frac{2r}{\alpha_+}\right)}{r^2} (r - r_-)^{1+\alpha} d\tilde{u} d\tilde{v}, \quad (37)$$

Similarly as $r \rightarrow r_-$,

$$dS_{RN}^2(r \rightarrow r_-) \rightarrow -\frac{\exp\left(\frac{2r}{\alpha_-}\right)}{r^2} (r_+ - r)^{1+\bar{\alpha}} d\tilde{u} d\tilde{v}, \quad (38)$$

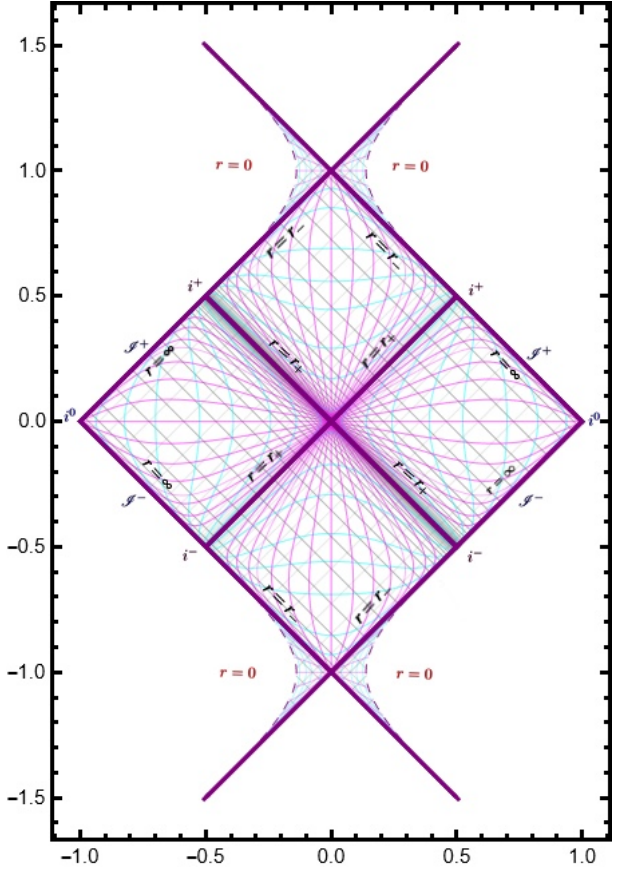


FIG. 5. Penrose Diagram for a block of Reissner Nordstrom ($M = 1$, $Q = .96$) Universes. The Kruskal coordinates (T, R) are plotted on the y-axis and x-axis respectively. The constant- r and constant- t curves are plotted in cyan and magenta while the null-geodesics are plotted in gray. The outer r_+ and inner r_- horizons are described by $T = \pm R$ and $T = \pm R \pm 1$ lines. While the physical singularity at $r = 0$ is plotted as a dashed purple curve.

However, this is not the end of the story. Similar to the Schwarzschild case, the Jacobian and its higher-order relatives will be undefined at the horizons, thus it is not straightforward to take the derivatives of the conformal factor implicitly. This is some kind of warning to the reader to avoid inferring that the modulus invoked in equation (36) means that the metric is not differentiable there. At the end of the day, the Jacobian itself is ill-defined or invertible near to the horizons. In other words, to check the differentiability of the metric in these coordinates, the metric should be fully written in terms of the CCG Kruskal coordinate first, as this will invoke generalized Lambert functions. This might be easier to handle numerically. However, no matter if these kinks cause a non-differentiability of the metric or not near the horizons, we can always get rid of them; for instance via the use of relaxation functions.

In short, another set of coordinates (\tilde{u}, \tilde{v}) can be introduced which will inherit the properties mentioned above

and possess a relaxed (without Kinks) conformal factor at r_+ and r_- . As a consequence, the metric will be guaranteed to be C^∞ if these Kinks were the only problem in these old coordinates. We list the relaxed version of the example of type-I in Appendix B. Before we move to construct the type-II coordinates $\mathcal{GK}_{\mathcal{II}}$, there are two features of the metric worth commenting on. First, the metric is not asymptotically flat and is different from the \mathcal{K}_\pm coordinates where the induced metric on the sub-manifold $M_2 = \mathcal{M} \setminus SO(3)$ is asymptotically vanishing. In $\mathcal{GK}_{\mathcal{I}}$ coordinates the induced metric on M_2 blows up. This is completely natural as the coordinates are compact, hence the proper distances is invariant. Second, the $\mathcal{GK}_{\mathcal{I}}$ coordinates are dynamically casting [46, 47] the metric since the conformal factor includes explicit time dependence after and before the relaxation. This prevents the r and t from being related to (\tilde{u}, \tilde{v}) by simple transformation similar to (18, 21).

B. Type-II Global Chart

While constructing $\mathcal{GK}_{\mathcal{I}}$, a simple zero at each horizon r_\pm was a coupled one at the other horizon r_\mp . This product of zeros had a semi-positive regular amplitude everywhere as shown in equation (36) or (B2). However, for $\mathcal{GK}_{\mathcal{II}}$ we will have a different singularity structure that serves the same purpose: sum of two zeros at each horizon r_\pm , each coupled to a semi-positive singular amplitude at the other horizon r_\mp that is singular at the other horizon. In principle, this class of charts should contain families of coordinates at which the coordinates themselves are extrapolation between the two Outer and Inner Kruksal coordinates. In light of this statement, the chart given in [1] plausibly belongs to that class, for more details look Appendix A.

The conformal metric will have a simple pole at $r = r_\pm$ coupled to $M_\pm(r_*, t)$, while $\beta(r_*, t)$ is effectively a residual term for completeness. $M_\pm(r_*, t)$ and $\beta(r_*, t)$ are satisfying the following constraints. As $r \rightarrow r_\pm$

$$\begin{aligned} M_\pm(r_*, t) &\rightarrow \text{constant}, \\ M_\mp(r_*, t) &\rightarrow 0, \\ \beta(r_*, t) &\rightarrow 0. \end{aligned} \tag{39}$$

Alternatively, we can restate the first constraint as: M_\pm must have no overall pole at r_+ (r_-). Later, through this analysis, we will learn that β will be the key to finding the global conformal charts in this procedure for the type-II coordinates. Given equation (15), we can rewrite this in

terms of the \mathcal{K}_\pm or the double null coordinates as follows

$$\begin{aligned} \frac{dh}{du} \frac{dk}{dv} &= \frac{\exp\left(\frac{2(r_* - r_+)}{\alpha_+}\right)}{|r - r_-|^\alpha} M_+(r_*, t) + \beta(r_*, t) \\ &+ \frac{\exp\left(-\frac{2(r_* - r_-)}{\alpha_-}\right)}{|r - r_+|^\alpha} M_-(r_*, t), \end{aligned} \tag{40}$$

Revisiting the condition in equation (39), M_+ (M_-) must have zeros at $r = r_-$ ($r = r_+$) of rank higher than α ($\bar{\alpha}$) respectively. Searching for solutions for equation (40) could be more fruitful if we were able to find functions M_\pm and β with $(r_* \pm t)$ dependence. Accordingly, the residual term β could be used to easily factorize the right-hand side of the equation (40) into a product of u - and v -dependent functions. The task of generating a solution to equation (40) is not trivial, but if we find $M_\pm(u, v)$ and $\beta(u, v)$, this will boost our progress towards achieving this task. The easiest hint we can get from the form of that equation is to try to construct $M_+(M_-)$ from the \mathcal{K}_+ (\mathcal{K}_-). Following this logic, using the trial and error method, we learn that if we define M_\pm as

$$\begin{aligned} M_+ &\equiv \frac{\mu_u \mu_v}{(1 + U_+^{1+2\bar{\alpha}})(1 + V_+^{1+2\bar{\alpha}})} \\ M_- &\equiv \frac{\mu_u \mu_v}{(1 + U_-^2)(1 + V_-^2)}, \end{aligned} \tag{41}$$

we can find β that can do the factorization for us

$$\beta \equiv \frac{\mu_u \mu_v U_+ V_-}{(1 + U_+^{1+2\bar{\alpha}})(1 + V_-^2)} + \frac{\mu_u \mu_v U_- V_+}{(1 + V_+^{1+2\bar{\alpha}})(1 + U_-^2)}. \tag{42}$$

This will leave us eventually with the following choices for $\frac{dh}{du}$ and $\frac{dk}{dv}$

$$\begin{aligned} \frac{dh}{du} &= \mu_u \left[\frac{U_+}{1 + U_+^{1+2\bar{\alpha}}} + \frac{U_-}{1 + U_-^2} \right] \\ \frac{dk}{dv} &= \mu_v \left[\frac{V_+}{1 + V_+^{1+2\bar{\alpha}}} + \frac{V_-}{1 + V_-^2} \right] \end{aligned} \tag{43}$$

We can also integrate these ODEs in terms of the hypergeometric and arctan functions.

$$\begin{aligned} S_\pm(x) &= \alpha_- \tan^{-1} \left(e^{\frac{x}{\alpha_-}} \right) \\ &+ \bar{\alpha}_\pm e^{\frac{x}{\alpha_\pm}} {}_2F_1(1, 1 - \bar{k}_\pm, 2 - \bar{k}_\pm, -e^{\bar{\kappa}x}) \end{aligned} \tag{44}$$

where

$$\begin{aligned} \bar{k}_\pm &= \frac{\bar{\alpha}_\pm}{\bar{\alpha}_+ + \bar{\alpha}_-} \\ \bar{\kappa} &= \frac{1}{\bar{\alpha}_-} + \frac{1}{\bar{\alpha}_+} \\ \bar{\alpha}_- &= \frac{\alpha_-}{2} \\ \bar{\alpha}_+ &= \alpha_+ \end{aligned} \tag{45}$$

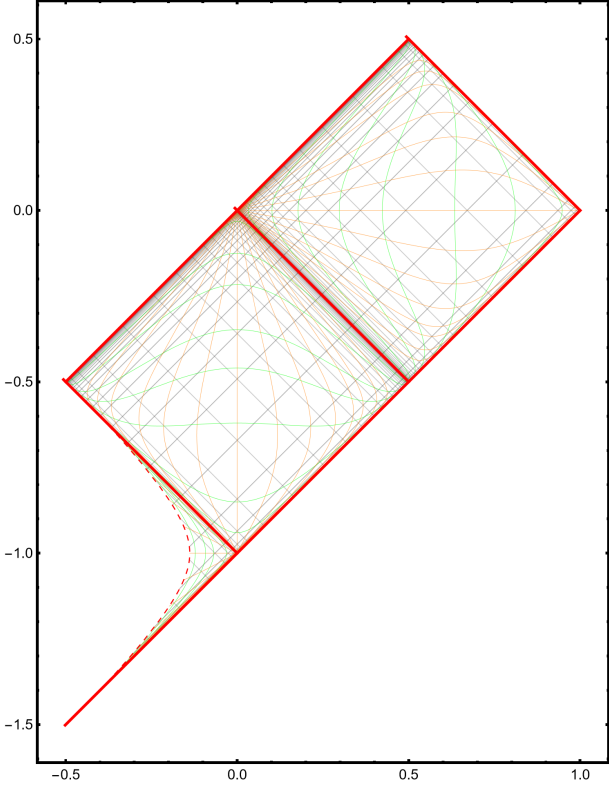


FIG. 6. Penrose Diagram for a single universe of Reissner Nordstrom ($M = 1$, $Q = .96$) Universes using type-II coordinates. The Kruskal coordinates (T, R) are plotted on the y -axis and x -axis respectively. The constant- r and constant- t curves are plotted in green and orange while the null-geodesics are plotted in gray. The outer r_+ and inner r_- horizons are described by $T = R$ and $T = -R - 1$ lines. While the physical singularity at $r = 0$ is plotted as a red curve.

The definition for the (\tilde{u}, \tilde{v}) follows in the same way as type-I ones in (32). One more time, the choice we made for $\mathcal{GK}_{\mathcal{I}\mathcal{I}}$ coordinates is naturally compact which means we can use these coordinates directly to build the Penrose diagrams. Again, our choice of the integration reference point will be the outer horizon r_+ . We can now write the metric

$$dS_{RN}^2 = -\frac{1}{r^2} \{ A_+^{-1}(r, t) + A_-^{-1}(r, t) + A^{-1}(r, t) \}^{-1} d\tilde{u} d\tilde{v} \quad (46)$$

where $A_{\pm}(r, t)$ and $A(r, t)$ are defined as follows

$$\begin{aligned} A_+(r, t) \equiv & \exp\left(-\frac{2r}{\alpha_+}\right) |r - r_-|^{\alpha+1} \\ & + \exp\left(\frac{2r}{\alpha_-}\right) |r - r_+|^{1+2\bar{\alpha}} |r - r_-|^{-1} \\ & + 2 \cosh\left[t\left(\frac{1}{\alpha_+} + \frac{2}{\alpha_-}\right)\right] \\ & \times \exp\left(r\left[-\frac{1}{\alpha_+} + \frac{2}{\alpha_-}\right]\right) |r - r_+|^{\bar{\alpha} + \frac{1}{2}} |r - r_-|^{\frac{\alpha}{2}} \end{aligned} \quad (47)$$

$$\begin{aligned} A_-(r, t) \equiv & \exp\left(\frac{2r}{\alpha_-}\right) |r - r_+|^{\bar{\alpha}+1} \\ & + \exp\left(-\frac{2r}{\alpha_-}\right) |r - r_-|^2 |r - r_+|^{-\bar{\alpha}+1} \\ & + 2 \cosh\left[\frac{2t}{\alpha_-}\right] |r - r_-| |r - r_+| \end{aligned} \quad (48)$$

$$\begin{aligned} A(r, t) \equiv & 2 \cosh[\kappa t] \exp(-\bar{\kappa}r) |r - r_+|^{\frac{1+\bar{\alpha}}{2}} |r - r_-|^{\frac{1+\alpha}{2}} \\ & + 2 \cosh[\bar{\kappa}t] \exp(-\kappa r) |r - r_+|^{\frac{1-\bar{\alpha}}{2}} |r - r_-|^{\frac{3+\alpha}{2}} \\ & + 2 \cosh\left[\frac{-t}{\alpha_-}\right] \exp\left(\frac{3r}{\alpha_-}\right) |r - r_+|^{\frac{2+3\bar{\alpha}}{2}} |r - r_-|^{\frac{-1}{2}} \\ & + 2 \cosh\left[\frac{-3t}{\alpha_-}\right] \exp\left(\frac{r}{\alpha_-}\right) |r - r_+|^{\frac{2+\bar{\alpha}}{2}} |r - r_-|^{\frac{1}{2}}, \end{aligned} \quad (49)$$

with the following limits

$$\begin{aligned} A_+(r \rightarrow r_+, t) & \rightarrow \exp\left(-\frac{2r}{\alpha_+}\right) |r - r_-|^{\alpha+1}, \\ A_-(r \rightarrow r_-, t) & \rightarrow \exp\left(\frac{2r}{\alpha_-}\right) |r - r_+|^{\bar{\alpha}+1}, \\ A_{\pm}(r \rightarrow r_{\mp}, t) & \rightarrow \infty, \\ A(r \rightarrow r_{\pm}, t) & \rightarrow \infty. \end{aligned} \quad (50)$$

Consequently, the metric will take the following asymptotic limit

$$\begin{aligned} dS_{RN}^2(r \rightarrow r_+) & = -\frac{e^{\frac{-2r}{\alpha_+}} |r - r_-|^{1+\alpha}}{r^2} d\tilde{u} d\tilde{v}, \\ dS_{RN}^2(r \rightarrow r_-) & = -\frac{e^{\frac{2r}{\alpha_-}} |r - r_+|^{1+\bar{\alpha}}}{r^2} d\tilde{u} d\tilde{v}. \end{aligned} \quad (51)$$

V. DISCUSSION AND CONCLUSION

After reinterpreting the premises of the Kruskal charting of the Schwarzschild spacetime, we were able to provide a new approach to chart the Reissner–Nordström spacetime featuring two horizons. The technique itself showed to be employable in two distinctive ways, resulting in two families of charting systems: conformal global *type-I* and *type-II* charts. In both cases, the asymptotic form of the metric approaches the form of metric written in terms of *Type-O* charts. We illustrated the success of the provided technique by constructing compact conformal global coordinates of type-I $\mathcal{GK}_{\mathcal{I}}$ and of type-II $\mathcal{GK}_{\mathcal{I}\mathcal{I}}$ for the RN spacetime. The price we pay for covering the whole spacetime with two horizons with only one chart is time dependence [46, 47].

After the construction, for both type-I and type-II charts, the metric becomes C^∞ if the kinks in the conformal factor near the horizons cause any ill-differentiability through the extra *relaxation* step in the procedure, we

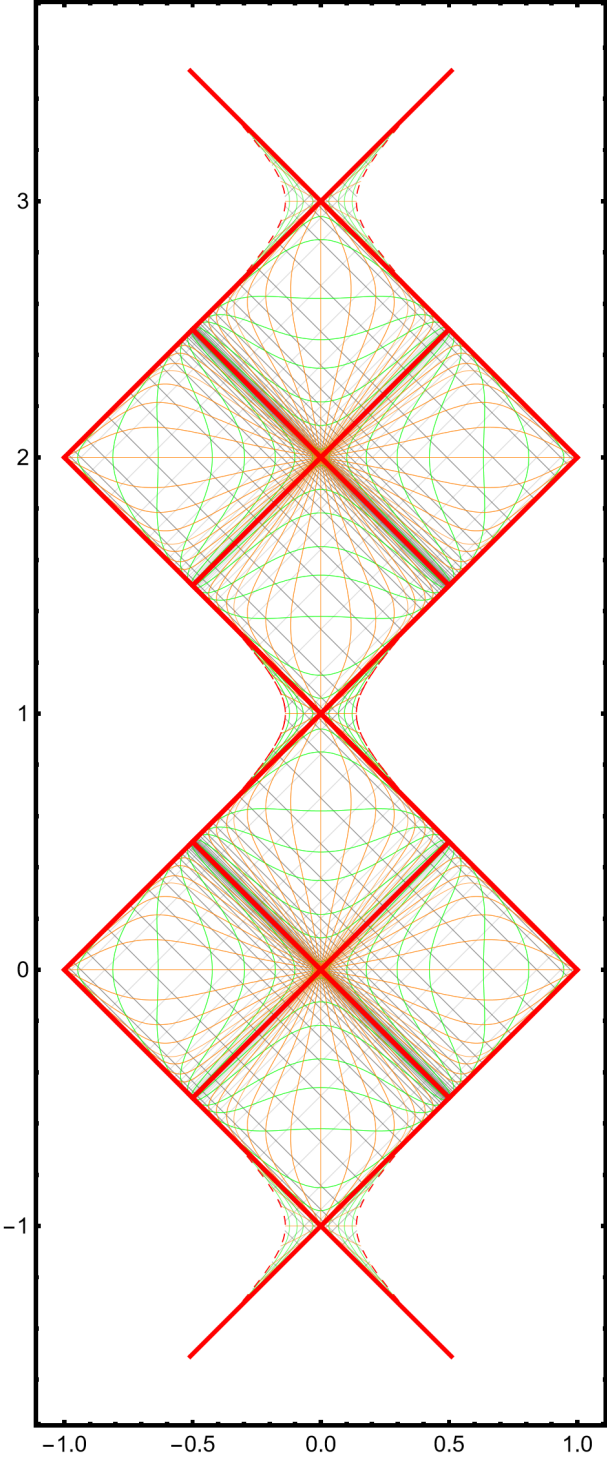


FIG. 7. Penrose Diagram for a maximal analytical extension of Reissner Nordstrom ($M = 1, Q = .96$) using type-II coordinates. The Kruskal coordinates (T, R) are plotted on the y -axis and x -axis respectively. The constant- r and constant- t curves are plotted in green and orange while the null-geodesics are plotted in gray. The outer r_+ and inner r_- horizons are described by $T = \pm R \pm \text{constant}$ and $T = \pm R \pm 1 \pm \text{constant}$ lines. While the physical singularity at $r = 0$ is plotted as a dashed red curve.

give an example of how to apply this step to the example of type-I chart in appendix B. As expected, it is complicated to write the generalized Kruskal coordinates (\tilde{u}, \tilde{v}) explicitly in terms of the RN coordinates (t, r) , related through equation (18, 21). However, we hinted that this could be achieved by utilizing the generalized Lambert function \mathcal{W} in similar manner to the use of the Lambert function W in Schwarzschild case.

For the charts we have provided of both types, we found that the Hypergeometric functions could be employed to map the non-global null coordinate to type-I and type-II CCG charts. Finally, we demonstrated that the smoothing technique developed in [1] could be thought of as a special case of the type II family of coordinates, as could be found in Appendix A. We believe that it is straightforward to apply this technique to spherical symmetric spacetimes with two horizons including non-strong spherical symmetric ones. Whether this procedure is applicable to glued spacetimes through thin shell approximation or to only the axial symmetric Kerr is fuzzy to authors and we believe separate and further analysis is required in order to answer such questions.

Appendix A: Soltanti's Smoothing Technique as Type-II

Following the notation in [1] and starting from equations (31-34), the metric could be written as follows

$$dS_{RN}^2 = \frac{(r - r_+)(r - r_-)}{r^2} dU dV \left\{ \frac{g_{\downarrow}(U)g_{\downarrow}(V)}{k_+^2 UV} + \frac{g_{\uparrow}(U)g_{\uparrow}(V)}{k_-^2(U-1)(V-1)} + \frac{M(U, V)}{k_+ k_-} \right\} + r^2 d\Omega^2 \quad (\text{A1})$$

where

$$\begin{aligned} M(U, V) &= M_1(U, V) + M_2(U, V) + M_3(U, V) \\ M_1(U, V) &= \frac{g_{\downarrow}(U)g_{\uparrow}(V)}{U(V-1)} + \frac{g_{\uparrow}(U)g_{\downarrow}(V)}{V(U-1)} \\ M_2(U, V) &= g'_{\downarrow}(U)g'_{\downarrow}(V) \ln|U| \ln|V| \\ &\quad + g'_{\uparrow}(U)g'_{\uparrow}(V) \ln|U-1| \ln|V-1| \\ &\quad + g'_{\uparrow}(U)g'_{\downarrow}(V) \ln|U-1| \ln|V| \\ &\quad + g'_{\downarrow}(U)g'_{\uparrow}(V) \ln|U| \ln|V-1| \\ M_3(U, V) &= g'_{\downarrow}(U) \left\{ \frac{g_{\downarrow}(V)}{V} + \frac{g_{\uparrow}(V)}{V-1} \right\} \ln|U| \\ &\quad + g'_{\uparrow}(U) \left\{ \frac{g_{\downarrow}(V)}{V} + \frac{g_{\uparrow}(V)}{V-1} \right\} \ln|U-1| \\ &\quad + g'_{\downarrow}(V) \left\{ \frac{g_{\downarrow}(U)}{U} + \frac{g_{\uparrow}(U)}{U-1} \right\} \ln|V| \\ &\quad + g'_{\uparrow}(V) \left\{ \frac{g_{\downarrow}(U)}{U} + \frac{g_{\uparrow}(U)}{U-1} \right\} \ln|V-1| \end{aligned} \quad (\text{A2})$$

First let us discuss the behaviour of M near the horizons. As we can see from figure [8] the M_2 function will be

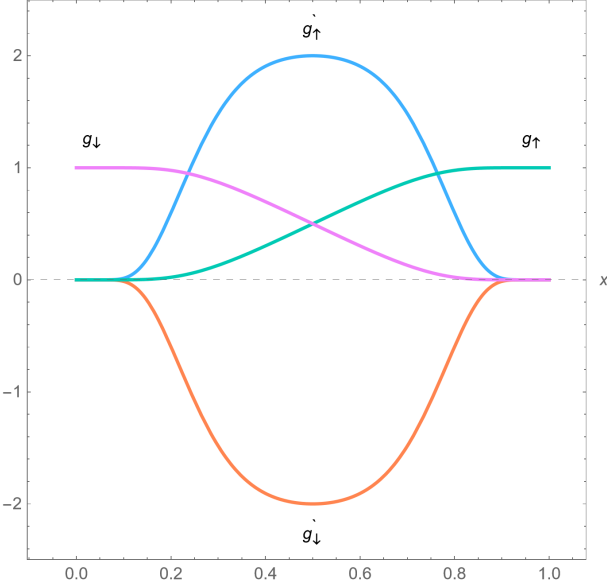


FIG. 8. the $g_{\uparrow}(x)$ and $g_{\downarrow}(x)$ and their derivatives of the $g'_{\uparrow}(x)$ and $g'_{\downarrow}(x)$.

vanishing near to each horizon which are located at 0, 1 of the coordinates $U(V)$. Similarly we can approximate equation (31-32) and only keeping the poles near each horizon to study the behaviour of M_1 , as $r \rightarrow r_+$

$$\begin{aligned} e^{k+u} &\simeq \frac{1}{U} \propto \frac{1}{|r-r_+|^{\frac{1}{2}} |r-r_-|^{\frac{-1}{2k_-}}} \\ e^{-k+v} &\simeq \frac{1}{V} \propto \frac{1}{|r-r_+|^{\frac{1}{2}} |r-r_-|^{\frac{-1}{2k_-}}} \end{aligned} \quad (\text{A3})$$

and as $r \rightarrow r_-$

$$\begin{aligned} e^{k-u} &\simeq \frac{1}{U-1} \propto \frac{1}{|r-r_-|^{\frac{1}{2}} |r-r_+|^{\frac{-1}{2k_+}}} \\ e^{-k-v} &\simeq \frac{1}{V-1} \propto \frac{1}{|r-r_-|^{\frac{1}{2}} |r-r_+|^{\frac{-1}{2k_+}}} \end{aligned} \quad (\text{A4})$$

Consequently, the product of $h(r)M_1$ is extrapolating to zero near to each horizon. Finally, a similar argument applies to $h(r)M_3$ with the extra piece of information that $g'_{\downarrow(\uparrow)}(x)$ growth rate is exponential approach the zero near the horizons which will overwhelm the $\ln|U(V)|$ blowing up there, thus this product will also extrapolate to zero near horizons. Accordingly, $h(r)M \rightarrow 0$ in agreement to the conditions we imposed on type-II coordinate β function.

Based on equations (A3, A4), it is easy to show that the terms $\frac{1}{UV}$ and $\frac{1}{(U-1)(V-1)}$ will follow the behaviour imposed on M_{\pm} .

.

Appendix B: Relaxed Version of Type-I CCG example

We choose the function $\tanh x$ to do this job. The relaxed coordinate transformation is

$$\begin{aligned} \frac{dh}{du} &= \frac{\mu_u}{\tanh[U_-^2] U_+^{-1} + \tanh[U_+^2] U_-^{-1}}, \\ \frac{dk}{dv} &= \frac{\mu_v}{\tanh[V_-^2] V_+^{-1} + \tanh[V_+^2] V_-^{-1}}. \end{aligned} \quad (\text{B1})$$

The metric now becomes

$$\begin{aligned} dS_{RN}^2 = -\mu_u \mu_v \frac{d\tilde{u} d\tilde{v}}{r^2} &\left\{ Q_-(r, t) |r - r_-|^{\alpha+1} \exp\left(-\frac{2r}{\alpha_+}\right) \right. \\ &+ Q_+(r, t) |r - r_+|^{\bar{\alpha}+1} \exp\left(\frac{2r}{\alpha_-}\right) \\ &\left. + \tilde{Q}(r, t) \exp\left(r \left[\frac{-1}{\alpha_+} + \frac{1}{\alpha_-}\right]\right) \frac{|r - r_+|^{\frac{\bar{\alpha}+1}{2}}}{|r - r_-|^{-\frac{\alpha+1}{2}}} \right\}, \end{aligned} \quad (\text{B2})$$

where Q_- , Q_+ , and \tilde{Q} are defined as

$$\begin{aligned} Q_-(r, t) &= \tanh \left[\exp\left(\frac{2(t-r)}{\alpha_-}\right) \frac{|r - r_-|}{|r - r_+|^{\bar{\alpha}}} \right] \\ &\times \tanh \left[\exp\left(\frac{-2(t+r)}{\alpha_-}\right) \frac{|r - r_-|}{|r - r_+|^{\bar{\alpha}}} \right] \\ Q_+(r, t) &= \tanh \left[\exp\left(\frac{2(r-t)}{\alpha_+}\right) \frac{|r - r_+|}{|r - r_-|^{\alpha}} \right] \\ &\times \tanh \left[\exp\left(\frac{-2(-t+r)}{\alpha_+}\right) \frac{|r - r_+|}{|r - r_-|^{\alpha}} \right] \\ \tilde{Q}(r, t) &= Q_1(r, t) \exp\left(t \left(\frac{1}{\alpha_+} + \frac{1}{\alpha_-}\right)\right) \\ &+ Q_2(r, t) \exp\left(-t \left(\frac{1}{\alpha_+} + \frac{1}{\alpha_-}\right)\right) \\ Q_1(r, t) &= \tanh \left[\exp\left(\frac{2(t-r)}{\alpha_-}\right) \frac{|r - r_-|}{|r - r_+|^{\bar{\alpha}}} \right] \\ &\times \tanh \left[\exp\left(\frac{-2(-t+r)}{\alpha_+}\right) \frac{|r - r_+|}{|r - r_-|^{\bar{\alpha}}} \right] \\ Q_2(r, t) &= \tanh \left[\exp\left(\frac{-2(t+r)}{\alpha_-}\right) \frac{|r - r_-|}{|r - r_+|^{\bar{\alpha}}} \right] \\ &\times \tanh \left[\exp\left(\frac{2(r-t)}{\alpha_+}\right) \frac{|r - r_+|}{|r - r_-|^{\alpha}} \right] \end{aligned} \quad (\text{B3})$$

This relaxed version of the conformal factor is guaranteed to be without any kinks everywhere in coordinates (\tilde{u}, \tilde{v}) . The integral I_2 defining (\tilde{u}, \tilde{v}) is given by

$$I_2 = \int \frac{dx}{\tanh(x^2) x^{q+1} + \tanh(x^{-2q})}, \quad (\text{B4})$$

The $q > 1$ cases could be evaluated numerically, however, analytical methods could still be helpful in studying the relation between \mathcal{K}_{\pm} and $\mathcal{G}\mathcal{K}_{\mathcal{T}}$ at any point. This

could be achieved for example by employing series expansion, as mentioned earlier. Moreover, if we manage to invert equations (B1) to solve explicitly for the null coordinates in terms of $\mathcal{GK}_{\mathcal{I}}$, then we could employ the generalized Lambert function to solve for (t, r) explicitly as well. Such an expansion is expected to recover equations (21) and (18) near to the horizons $r = r_-$ and $r = r_+$, respectively.

ACKNOWLEDGMENTS

We express our sincere gratitude to Dr. Wei-Chen Lin¹² for his invaluable guidance and unwavering support throughout the duration of this project and also for

sharing his own resources for plotting Penrose diagrams. Our appreciation also extends to Dr. Joseph Schindler¹³, Mahmoud Mansour¹⁴, and their insightful contributions to various aspects of the analysis presented in this article. We extend special thanks to Dr. Sam Powers for providing invaluable comments on the draft, and our appreciation to Professor William H. Kinney for sharing insightful perspectives on how we can plot the Penrose diagrams. The visual richness of this work owes much to the artistic talents of Haidi Fawzi¹⁵, whose illustrations greatly enhance the overall presentation. We owe Haidi Fawzi a considerable debt of thanks. Additionally, we acknowledge the partial support of Dr. D.S. by the US National Science Foundation under Grants No. PHY-2014021 and PHY-2310363.

[1] Farshid Soltani. Global kruskal-szekeres coordinates for reissner-nordström spacetime, 2023. [arXiv:2307.11026](https://arxiv.org/abs/2307.11026).

[2] Jonatan Nordebo. the reissner nordström metric, Mar 2016. URL: <https://www.semanticscholar.org/paper/The-Reissner-Nordstr%C3%B6m-metric-Nordebo/9311976210064b18e4f59223665cdb14cffb6c26>.

[3] Sean M. Carroll. *Spacetime and Geometry: An Introduction to General Relativity*. Cambridge University Press, Jan 2003.

[4] Jerry B. Griffiths and Jiří Podolský. *Exact Space-Times in Einstein's General Relativity*. Cambridge University Press, Aug 2012.

[5] Matthias Blau. General relativity lecture notes. URL: <http://www.blau.itp.unibe.ch/Lecturenotes.html>.

[6] Subrahmanyan Chandrasekhar. *The Mathematical Theory of Black Holes*. Clarendon Press, Jan 1983.

[7] Matt Visser. The kerr spacetime: A brief introduction. *arXiv*, 2008. doi:10.48550/arXiv.0706.0622.

[8] Saul A. Teukolsky. The kerr metric, Jan 2015. URL: <https://arxiv.org/abs/1410.2130>.

[9] Charles W. Misner, K. S. Thorne, and J. A. Wheeler. *Gravitation*. W. H. Freeman, San Francisco, 1973.

[10] I. D. Novikov. *Early Stages of the Evolution of the Universe (Doctoral Dissertation)*. PhD thesis, Sternberg Astronomical Institute, Moscow, 1963.

[11] Abbé Georges Lemaître. The expanding universe. *General Relativity and Gravitation*, 29(5):641–680, 1997. doi:10.1023/a:1018855621348.

[12] Karl Martel and Eric Poisson. Regular coordinate systems for schwarzschild and other spherical spacetimes. *American Journal of Physics*, 69(4):476–480, 2001. doi:10.1119/1.1336836.

[13] Howard P. Robertson and Thomas W. Noonan. *Relativity and cosmology*. Saunders, 1969.

[14] David Finkelstein. Past-future asymmetry of the gravitational field of a point particle. *Physical Review*, 110(4):965–967, 1958. doi:10.1103/physrev.110.965.

[15] M. D. Kruskal. Maximal extension of schwarzschild metric. *Physical Review*, 119(5):1743–1745, 1960. doi:10.1103/physrev.119.1743.

[16] W. G. Unruh. Global coordinates for schwarzschild black holes. URL: <http://www.theory.physics.ubc.ca/530-21/bh-coords2.pdf>.

[17] José P.S. Lemos and Diogo L.F.G. Silva. Maximal extension of the schwarzschild metric: From painlevé–gullstrand to kruskal–szekeres. *Annals of Physics*, 430:168497, jul 2021. URL: <https://doi.org/10.1016%2Fj.aop.2021.168497>, doi:10.1016/j.aop.2021.168497.

[18] Manuela Campanelli, Gaurav Khanna, Pablo Laguna, Jorge Pullin, and Michael P Ryan. Perturbations of the kerr spacetime in horizon-penetrating coordinates. *Classical and Quantum Gravity*, 18(8):1543–1554, 2001. doi:10.1088/0264-9381/18/8/310.

[19] Francesco Sorge. Kerr spacetime in lemaître coordinates. *Arxiv*, Jan 2022. doi:arXiv:2112.15441.

[20] Cosimo Bambi. Astrophysical black holes: A review. *Proceedings of Multifrequency Behaviour of High Energy Cosmic Sources - XIII — PoS(MULTIF2019)*, 2020. doi:10.22323/1.362.0028.

[21] Michal Zajaček and Arman Tursunov. Electric charge of black holes: Is it really always negligible?, 2019. arXiv:1904.04654.

[22] Vitor Cardoso, Caio F.B. Macedo, Paolo Pani, and Valeria Ferrari. Black holes and gravitational waves in models of minicharged dark matter. *Journal of Cosmology and Astroparticle Physics*, 2016(05):054–054, may 2016. URL: <https://doi.org/10.1088%2F1475-7516%2F2016%2F05%2F054>, doi:10.1088/1475-7516/2016/05/054.

[23] De-Chang Dai, Katherine Freese, and Dejan Stojkovic. Constraints on dark matter particles charged under a hidden gauge group from primordial black holes. *JCAP*, 06:023, 2009. arXiv:0904.3331, doi:10.1088/1475-7516/2009/06/023.

[24] Andrew J. S. Hamilton. General relativity, black holes and cosmology, Jan 2020. URL: https://jila.colorado.edu/~ajsh/astr3740_17/grbook.pdf.

[25] Thomas Klösch and Thomas Strobl. Classical and quantum gravity in 1 + 1 dimensions. ii: The universal coverings. *Classical and Quantum Gravity*, 13(9):2395–2421,

¹² ArchennLin[AT]gmail.com

¹³ jcschindler01[AT]gmail.com

¹⁴ mansour[AT]iis.u-tokyo.jp.ac

¹⁵ behance.net/haidyfawzi?

sep 1996. URL: <https://doi.org/10.1088%2F0264-9381%2F13%2F9%2F007>, doi:10.1088/0264-9381/13/9/007.

[26] B. Carter. The complete analytic extension of the Reissner-Nordström metric in the special case $e^2 = m^2$. *Physics Letters*, 21(4):423–424, jun 1966. URL: <https://ui.adsabs.harvard.edu/abs/1966PhL....21..423C>, doi:10.1016/0031-9163(66)90515-4.

[27] John C. Graves and Dieter R. Brill. Oscillatory character of reissner-nordström metric for an ideal charged wormhole. *Phys. Rev.*, 120:1507–1513, Nov 1960. URL: <https://link.aps.org/doi/10.1103/PhysRev.120.1507>, doi:10.1103/PhysRev.120.1507.

[28] Wei-Chen Lin and Dong-han Yeom. Matching Radial Geodesics in Two Schwarzschild Spacetimes (e.g. Black-to-White Hole Transition) or Schwarzschild and de Sitter Spacetimes (e.g. Interior of a Non-singular Black Hole). 4 2023. [arXiv:2304.01654](https://arxiv.org/abs/2304.01654).

[29] Francesco Fazzini, Carlo Rovelli, and Farshid Soltani. Painlevé-gullstrand coordinates discontinuity in the quantum oppenheimer-snyder model. *Physical Review D*, 108(4), 2023. doi:10.1103/physrevd.108.044009.

[30] John M. Lee. *Introduction to Smooth Manifolds*. Springer, Sep 2002.

[31] Loring W. Tu. *An Introduction to Manifolds*. Springer, Aug 2008.

[32] J C Schindler and A Aguirre. Algorithms for the explicit computation of penrose diagrams. *Classical and Quantum Gravity*, 35(10):105019, apr 2018. URL: <https://doi.org/10.1088%2F1361-6382%2Faabce2>, doi:10.1088/1361-6382/aabce2.

[33] Joseph C. Schindler, Anthony Aguirre, and Amita Kuttner. Understanding black hole evaporation using explicitly computed penrose diagrams. *Physical Review D*, 101(2), jan 2020. URL: <https://doi.org/10.1103%2Fphysrevd.101.024010>, doi:10.1103/physrevd.101.024010.

[34] J. C. Schindler. *The Structure of Evaporating Black Holes (Doctoral Dissertation)*. PhD thesis, UNIVERSITY OF CALIFORNIA, SANTA CRUZ, 2019.

[35] Rosa Doran, Francisco S. N. Lobo, and Paulo Crawford. Interior of a schwarzschild black hole revisited. *Foundations of Physics*, 38(2):160–187, dec 2007. URL: <https://doi.org/10.1007%2Fs10701-007-9197-6>, doi:10.1007/s10701-007-9197-6.

[36] A Romadani and M F Rosyid. Kruskal-szekeres coordinates of spherically symmetric solutions in theories of gravity. *Journal of Physics: Conference Series*, 1816(1):012030, feb 2021. URL: <https://dx.doi.org/10.1088/1742-6596/1816/1/012030>, doi:10.1088/1742-6596/1816/1/012030.

[37] Valeri P. Frolov and Igor D. Novikov. *Black hole physics : basic concepts and new developments*, volume 96. Springer Netherlands, Jan 1998. doi:10.1007/978-94-011-5139-9.

[38] Fawzi. A. Generalized Kruskal Coordinate Notebook, 2023. URL: tobeupdated.

[39] Robert M. Wald. *General Relativity*. Chicago Univ. Pr., Chicago, USA, 1984. doi:10.7208/chicago/9780226870373.001.0001.

[40] Robert M. Corless, Gaston H. Gonnet, D. E. G. Hare, David J. Jeffrey, and Donald E. Knuth. On the lambert w function. *Advances in Computational Mathematics*, 5(1), Dec 1996. doi:10.1007/BF02124750.

[41] Thomas Mueller and Frank Grave. Catalogue of spacetimes, 2010. [arXiv:0904.4184](https://arxiv.org/abs/0904.4184).

[42] Istvan Mezo and Arpad Baricz. On the generalization of the lambert w function. *Transactions of the American Mathematical Society*, 369(11):7917–7934, 2017. doi:10.1090/tran/6911.

[43] István Mező, Cristina B Corcino, and Roberto B Corcino. Resolution of the plane-symmetric einstein-maxwell fields with a generalization of the lambert w function. *Journal of Physics Communications*, 4(8):085008, 2020. doi:10.1088/2399-6528/abab40.

[44] István Mező and Grant Keady. Some physical applications of generalized lambert functions. *European Journal of Physics*, 37(6):065802, 2016. doi:10.1088/0143-0807/37/6/065802.

[45] Tony C. Scott, Robert Mann, and Roberto E. Martinez II. General relativity and quantum mechanics: Towards a generalization of the lambert w function a generalization of the lambert w function. *Applicable Algebra in Engineering, Communication and Computing*, 17(1):41–47, 2006. doi:10.1007/s00200-006-0196-1.

[46] Wei-Chen Lin. private communication.

[47] Wei-Chen Lin, Dejan Stojkovic, and Dong han Yeom. Trouble with the penrose diagram in spacetimes connected via a spacelike thin shell, 2023. [arXiv:2302.04923](https://arxiv.org/abs/2302.04923).

[48] A. Ronveaux. *Heun's differential equations*. Oxford University press, 2007.

[49] Hypergeometric function. URL: <https://mathworld.wolfram.com/HypergeometricFunction.html>.

[50] Chapter 15 hypergeometric function. URL: <https://dlmf.nist.gov/15>.